JOURNAL OF CATALYSIS 83, 205–224 (1983)

Diffusion and Reaction in Blocked and High Occupancy Zeolite Catalysts

DOROS THEODOROU AND JAMES WEI

Department of Chemical Engineering, Massachusetts Institute of Technology, Cambridge, Massachusetts 02139

Received November 30, 1982; revised April 11, 1983

Diffusion in a ZSM-5 zeolite crystal is modeled as a simple random walk process in a finite, two-dimensional network of pores. Pore blocking is investigated as a model for catalyst modifications to enhance shape selectivity. The effects of random blocking of pores in the bulk of the crystal, or of pore entrances along the crystal border, are examined quantitatively. The behavior of effective intracrystalline diffusivity vs percentage of pores blocked is highly dependent on the blocking mode. A Monte-Carlo model for diffusion and reaction in a zeolite crystal is developed to study the effects of intracrystalline occupancy by gaseous molecules on the degree of diffusional effects on the reaction. For the simple isomerization A $\rightleftharpoons$ B, where species A and B have equal diffusivities, results obtained by Monte-Carlo simulation deviate from the predictions of a corresponding continuum approach in the region of high occupancies. This is due to the "finiteness" of the crystal, which is incorporated in the stochastic model, but not accounted for in the continuum approach.

INTRODUCTION

Zeolite structure is characterized by the presence of regular systems of intracrystalline cavities and pores, whose diameter lies in the range 3–10 Å, i.e., is commensurable with ordinary molecular dimensions (*1*).

A fascinating structure-related aspect of zeolite catalysis is molecular shape selectivity (*2, 3*). The subtle interplay of "configurational" diffusion and intrinsic kinetics in the intracrystalline pore system enables zeolite catalysts to "differentiate" between molecules or transition states involved in a reaction on the basis of their size and shape, and direct the reaction along specific paths.

Alkyl aromatic transformations over the zeolite ZSM-5, such as toluene disproportionation, alkylation of toluene with methanol, and xylene isomerization, in which mixtures of xylene isomers are produced, exhibit *para*-selectivity (*4–7*). *Para*-selective forms of the ZSM-5 have yielded product mixtures containing as much as 97% *para*-isomer to total xylenes, in large excess of the equilibrium composition of approximately 23% *ortho*-, 54% *meta*-, and 24% *para*-xylene (327°C) (*4*). A plausible explanation of *para*-selective phenomena can be based on the much higher intracrystalline diffusivity of *para*-xylene in relation to the other two isomers (*7, 8*). *Para*-xylene formed by the catalytic reaction can readily escape through the pore system, while the other two isomers linger in the pores and further isomerize to the more mobile *para*-xylene. A quantitative diffusional theory of *para*-selectivity was presented by Wei (*8*). Assuming a xylene isomerization rate matrix consistent with the observed equilibrium composition, and a ratio of diffusivities 1 : 1 : 1000 for $o : m : p$-xylene, respectively, this theory succeeds in predicting data from *para*-selective catalysts with very good accuracy.

On the basis of the diffusional explanation, a necessary condition for *para*-selectivity to be observed is that the situation in the zeolite catalyst be *diffusion limited.*

According to current views, ordinary (unmodified, small crystal) HZSM-5 does not exhibit pronounced *para*-selective properties at low temperatures. Tremen-

0021-9517/83 $3.00

dous enhancement of *para*-selectivity is observed when the catalyst undergoes certain modifications, such as coking (*4, 9*), treatment with phosphorus compounds (*4, 10*), impregnation with boron (*4, 6*), or magnesium (*6, 7*) compounds, and surface coating with polymers (*4*). In addition, large crystal HZSM-5 displays a moderately *para*-selective behavior (*7*).

Catalyst modifications probably result in structural changes of the intracrystalline channel system, such as pore blocking. The accompanying increase in *para*-selectivity could be attributed, in the spirit of the diffusional theory, to an increase in "tortuosity" of the path which diffusing molecules must follow in the modified catalyst crystal (*2*). Retardation of intracrystalline transport in the presence of blockings could bring a reaction originally free of diffusional limitations into the diffusion-controlled regime. Indeed, experimental results (*11*) show a drop in xylene diffusivity upon catalyst modification. Direct experimental evidence on the relation between intracrystalline diffusivity and selectivity toward *p*-xylene has been presented by Haag and Olson (*2*).

Another factor, which would be expected to affect the reaction–diffusion regime in a zeolite crystal is *occupancy* of the channel system by sorbed reactant and product molecules. Under ordinary operating conditions (1–10 atm, >350°C), occupancy is quite low. (At 1 atm, 538°C, Haag *et al.* (*12*) estimate the average distance between sorbed molecules as 400 Å, i.e., greater than 50 molecular diameters.) It is conceivable that, under conditions of higher pressures and lower temperatures, or operation in the liquid phase, significant occupancies can be achieved. At high occupancies, interference between "sorbed" molecules, acting as "mobile blockings" in the zeolite pores, would be expected to retard intracrystalline mass transport, bringing the reaction into a diffusion-limited regime. This would result in *para*-selectivity, even in the unmodified HZSM-5 catalyst.

The purpose of this work is to examine theoretically some factors that may lead to a diffusion-limited situation in zeolite catalysis. An elementary quantification of the relationship between aspects of zeolite structure and catalytic properties is thus attempted. The work presented is divided into three sections:

(I) Theoretical examination of the effects of pore blocking on the effective diffusivity in the crystal.

(II) Theoretical examination of the effects of intracrystalline occupancy on the catalytic reaction–diffusion regime.

(III) Modeling the reaction and diffusion situation in a partially blocked crystal.

The approach used in a large part of the modeling work is stochastic in character.

I. EFFECTS OF PORE BLOCKING IN INTRACRYSTALLINE DIFFUSIVITY

The zeolite crystal is modeled here as a finite, two-dimensional rectangular grid of intersecting channels, as shown in Fig. 1. Pore segments between successive intersections, or "sites," are considered as having equal length. This grid is doubtlessly a drastic oversimplification of the actual three-dimensional ZSM-5 channel network (*3, 13, 14*). Nevertheless, it retains the feature of regularity, typical of a crystalline structure, as well as the feature of interconnection of pores (coordination of each site $= 4 > 3$), which is considered critical in determining the concentration dependence of diffusivity (*1*).

Computing time considerations limited the size of the grid used in the range 11×11 to 21×21. In reality, a plane section of a typical 1-μm ZSM-5 crystal along a (100) plane cuts through $10000/13.4 \simeq 750$ pores of the larger diameter parallel pore system. A similar section in a small, 0.02-μm crystal cuts through $200/13.4 \simeq 15$ pores. Thus, our grid size is more representative of small ZSM-5 crystals.

Intracrystalline transport is modeled as a two-dimensional *random walk* within the

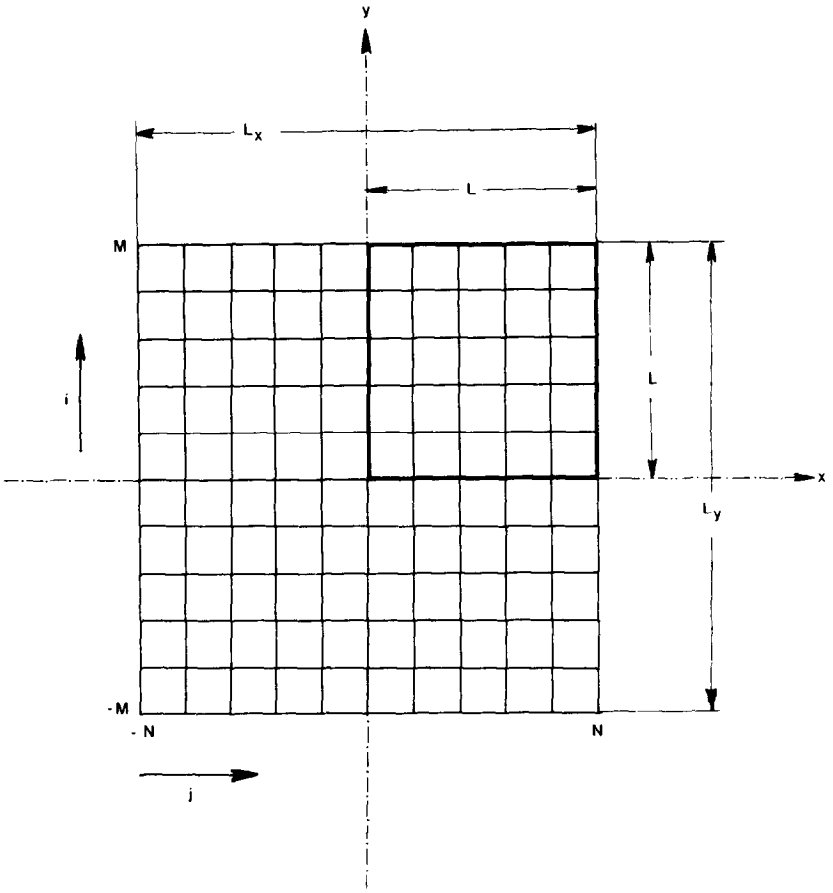

FIG. 1. Two-dimensional rectangular grid, used as a simple model of a zeolite crystal.

pore system. The following assumptions are made:

(*A.1*) Diffusion of a molecule is considered as a succession of discrete "steps," or jumps, from intersection to intersection. Only single steps, of length l, are considered. (In the real lattice, l would be of the order 10 Å.)

(*A.2*) In the absence of blocking or occupancy effects, the time interval between successive steps of a molecular species j is considered as constant and equal to τ_j.

(*A.3*) In the absence of blocking or occupancy effects, a molecule will move to one of the 4 adjacent sites with equal probability ($\frac{1}{4}$) at each step.

(*A.4*) Surface diffusion, considered to be important in zeolite catalysis, is accounted for, in an elementary way, by allowing lateral movement of molecules from site to site along the grid border.

The straight channels of 5.4 × 5.6 Å should give faster diffusion than the sinusoidal channels of 5.1 × 5.4 Å. The diffusion rate should also depend on the size of the diffusing molecule, and the interaction with the crystal structure. In this paper, we assume that the diffusion rates in the two sets of channels are equal. The time interval τ is related to the diffusion coefficient D and length l by the Brownian motion formula $l^2 = 4D\tau$. Since the diffusion coefficients in ZSM-5 at 315°C are 10^{-7} cm^2/sec for benzene and *p*-xylene, 10^{-10} cm^2/sec for *o*-xylene, and 10^{-12} cm^2/sec for 1,3,5-trimethylbenzene (*15*), the corresponding time intervals are $\tau = 5 \times 10^{-8}$, 5×10^{-5}, and 5×10^{-3} sec, respectively.

Additional assumptions, introduced in the investigation of pore blocking and occupancy effects, are described in the following.

Our simple random walk approach is comparable to the "jump" models that have been used in the literature to describe diffusion in the "cagelike" lattices of sorbent zeolites, such as zeolite A (*16–18*). In particular, assumption *A.3* implies that a diffusing molecule loses all memory of its direction at each step. In a system of interconnected channels, of diameter approximately equal to that of diffusing molecules, this could be a result of the force field experienced by the molecules at channel intersections, i.e., pore intersections are implicitly assumed to be sorption sites of equal strength. The idea that sorptive and catalytic activity of the ZSM-5 resides at pore intersections is common in the literature, and is in accordance with the fact that there is roughly a 1 to 1 correspondence between Al atoms in the lattice and pore intersections (*3, 19*).

The objective of our "pore-blocking" computer experiments is to determine a quantitative relation between effective diffusivity and extent of blocking. Two blocking modes are examined:

(a) Random blocking of pores in the interior, or "bulk" of the catalyst crystal. Bulk blocking is an appropriate model for modifications in which the species reacting to form the blockings is small enough, so that it can readily penetrate the crystal and cause structural changes in its entire mass. Thus, it may be suitable for describing modifications by Mg or B compounds.

(b) Random blocking of pore entrances along the crystal border. This blocking model is appropriate for modifications in which the species reacting to form the blockings is bulky, so that it penetrates the grid very slowly, or not at all, i.e., the modification reaction is severely diffusion limited. According to published experimental works, this condition seems to be satisfied in many cases of ZSM-5 modification by treatment with phosphorus compounds (*10*), surface coating with polymers, and even coking (*9*).

At the beginning of each random walk computer experiment a random blocking configuration, containing a predetermined number N_b of blocked pores, or pore entrances, is generated. We symbolize by x_b the fraction of total pores blocked. Once the grid topology is defined, the random walk of a single particle through it is stochastically modelled as follows:

At time $t = 0$ the particle is "placed" at the center of the grid, i.e., the following spatial probability distribution is accepted:

$$P_{i,j}^{(0)} = \delta(i) \cdot \delta(j) \qquad (-M \le i \le M,\ -N \le j \le N) \quad (1)$$

where $P_{i,j}^{(n)}$ denotes the probability of the particle being at position (i,j) at the nth random walk step and δ denotes the Dirac delta function.

The particle is subsequently allowed to diffuse through the grid, the probability distribution being updated at each step by use of the recursive relation:

$$P_{i,j}^{(n+1)} = P_{i,j-1}^{(n)} \cdot p_{i,j-1}^{R} + P_{i,j+1}^{(n)} \cdot p_{i,j+1}^{L} + P_{i-1,j}^{(n)} \cdot p_{i-1,j}^{U} + P_{i+1,j}^{(n)} \cdot p_{i+1,j}^{D} + P_{i,j}^{(n)} \cdot p_{i,j}^{S}. \quad (2)$$

Transition probabilities $p_{i,j}^{R}, p_{i,j}^{L}, p_{i,j}^{U}, p_{i,j}^{D}, p_{i,j}^{S}$, for moving to the right, to the left, up, down, or staying at the same place, respectively, are set as soon as the topology of the grid is defined. They satisfy the fundamental relation:

$$p_{i,j}^{R} + p_{i,j}^{L} + p_{i,j}^{U} + p_{i,j}^{D} + p_{i,j}^{S} = 1 \qquad (-M \le i \le M,\ -N \le j \le N). \quad (3)$$

For a totally unblocked grid, $p_{i,j}^{R} = p_{i,j}^{L} = p_{i,j}^{U} = p_{i,j}^{D} = \frac{1}{4}$ and $p_{i,j}^{S} = 0$.

The outside world is formally treated as two pairs of additional rows and columns of imaginary sites surrounding the crystal, from which there is no way back into the crystal:

$$p^{R}_{i,-(N+1)} = p^{L}_{i,(N+1)} = p^{U}_{-(M+1),j} = p^{D}_{(M+1),j} = 0. \quad (4)$$

The probability that the particle exits the grid is computed at each step. In this way, a functional relationship between the number of steps taken (n) and the probability of the particle being in the grid,

$$P^{(n)}_{in} = \sum_{i=-M}^{M} \sum_{j=-N}^{N} P^{(n)}_{i,j} \quad (5)$$

is "experimentally" determined.

In the case of a totally unblocked grid, one can show that our single particle random walk experiment is nothing more than a finite difference approximation to the two-dimensional continuum diffusion problem:

$$\frac{\partial P}{\partial t} = D\left(\frac{\partial^2 P}{\partial x^2} + \frac{\partial^2 P}{\partial y^2}\right) \quad (6)$$

$$P\left(-\frac{L_x}{2},y,t\right) = 0 \qquad P\left(\frac{L_x}{2},y,t\right) = 0$$

$$P\left(x,-\frac{L_y}{2},t\right) = 0 \qquad P\left(x,\frac{L_y}{2},t\right) = 0$$

$$P(x,y,0) = \begin{cases} 1, \text{ for } (x,y) = (0,0) \\ 0, \text{ everywhere else} \end{cases}$$

where $L_x = (2N + 2)\,l$, $L_y = (2M + 2)\,l$, $t = n\tau$. The effective diffusivity D is given in this case by the well-known formula

$$D = \frac{l^2}{4\tau} \quad (7)$$

The analytical solution to the continuum problem (6) is a Green's function, given by Carslaw and Jaeger (*20*). The quantity

$$P_{in}(t) = \int_{-L_x/2}^{L_x/2} \int_{-L_y/2}^{L_y/2} P(x,y,t)\,dxdy$$

is a continuum analogue of $P^{(n)}_{in}$, which can be expressed, by use of the continuum solution, as

$$P^{(n)}_{in,\,theoretical} = \left\{\frac{4}{\pi}\sum_{k_1=1}^{\infty}\frac{(-1)^{k_1}}{(2k_1-1)} \cdot \exp\left[-\left(\frac{D\tau}{l^2}\right)\pi^2\frac{(2k_1-1)^2}{4(N+1)^2}n\right]\right\} \cdot \left\{\frac{4}{\pi}\sum_{k_2=1}^{\infty}\frac{(-1)^{k_2}}{(2k_2-1)} \cdot \exp\left[-\left(\frac{D\tau}{l^2}\right)\pi^2\frac{(2k_2-1)^2}{4(M+1)^2}n\right]\right\}. \quad (8)$$

The latter is a theoretical relation between $P^{(n)}_{in}$ and n, which involves only the grid size (M,N) and the dimensionless effective diffusivity $\tilde{D} = D\tau/l^2$. An estimate of $\tilde{D}$ can be obtained by applying a least-squares fitting procedure of the theoretical Eq. (8) on the experimental results (5). In the case of a totally unblocked grid, the value of $\tilde{D}$ is, as would be expected, very close to the value 0.25 predicted by (7). If one assumes that intracrystalline transport in the presence of blockings can still be described by the diffusion Eq. (6), then one can define a dimensionless effective diffusivity, $\tilde{D}$, by applying the abovementioned fitting procedure to the random walk results in the blocked grid. The functionality $\tilde{D}(N_b)$, or, equivalently, $\tilde{D}(x_b)$, is a direct quantitative expression of the effects of structural modifications on intracrystalline transport rates.

a. Bulk Pore Blocking

In this blocking mode, pores to be blocked are chosen at random among the total number of $8MN - 2(M + N)$ internal and $4(M + N)$ surface pores of a $(2M + 1) \times (2N + 1)$ grid (a "pore" is defined here as the rectilinear segment between two adjacent nodes, or intersections). Some examples of random bulk pore blocking configurations created by our computer program in an 11×11 grid are given in Fig. 2 (lines denote blocked pores). There are 121 grid points, 180 internal pores, and 40 surface pores.

In mathematical terms, "blocking" im-

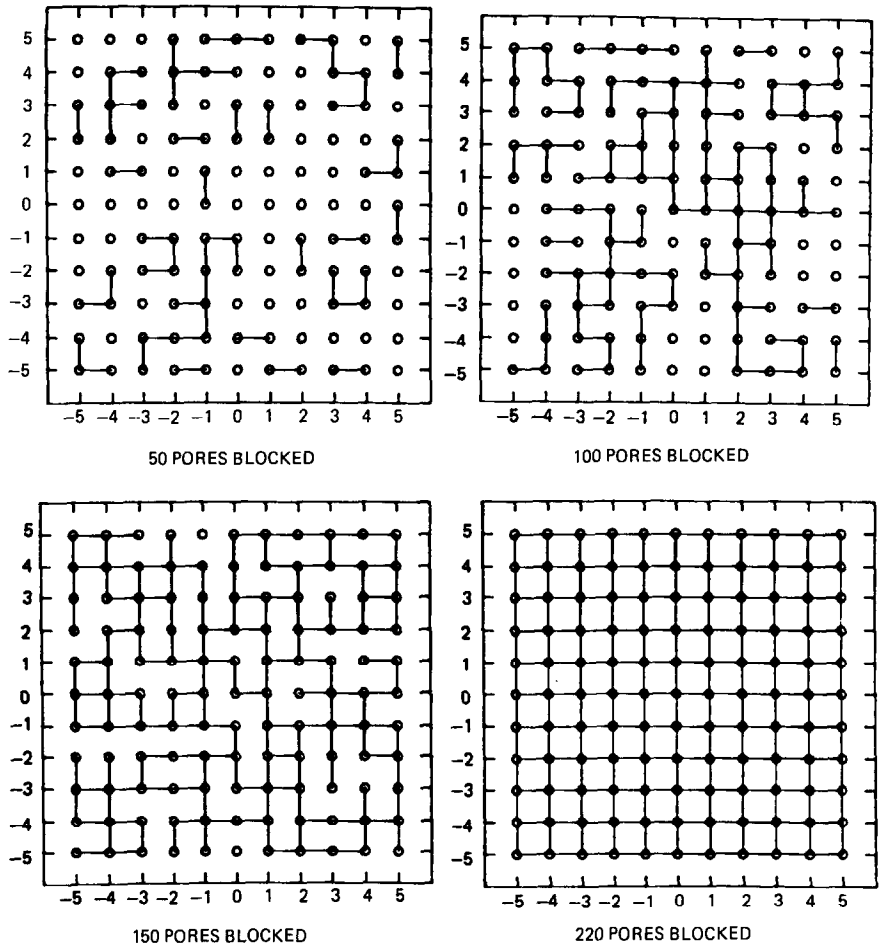

FIG. 2. Examples of random bulk pore blocking configurations in an 11 × 11 network.

plies a reduced transition probability for movement through a pore. A small value $b \ll \frac{1}{4}$ is accepted for the probability of movement of a particle from either end of a blocked pore to the other end. The probability of staying at the same place is increased by an amount $(\frac{1}{4} - b)$ at the two ends of a blocked pore, so that the fundamental relation (3) is everywhere satisfied. An elementary example is given in Fig. 3, to clarify assumptions as to the changes in transition probabilities brought about by bulk pore blocking. The probability distribution $P_{in}^{(n)}$, obtained from single particle random walk experiments, varies with the fraction of blocked pores (x_b), but also shows some dependence on the particular configuration of the grid, i.e., the exact location of the blocked pores. Thus, for each value of N_b, several blocking experiments are performed, to obtain averages and standard deviations in $\tilde{D}$. The latter are indi-

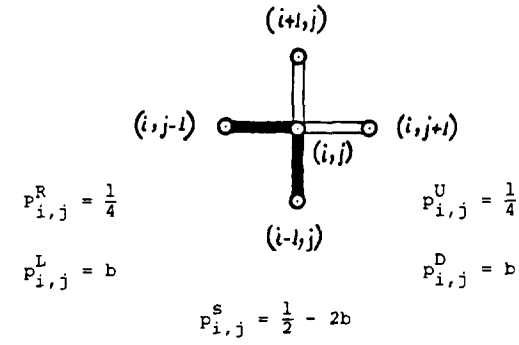

FIG. 3. Changes in transition probabilities brought about by bulk pore blocking.

cated by bars in the diagrams presented below.

Completely blocked pores correspond to a value of $b = 0$. However, use of this value at high extents of blocking may result in configurations which "trap" the diffusing molecule altogether. Use of a small, but finite value of b gives a smoother picture of the functionality $\tilde{D} = \tilde{D}(N_b)$.

The dependence of dimensionless diffusivity $\tilde{D} = D\tau/l^2$ on bulk pore blocking, as determined in a grid with $M = N = 10$, using a value of $b = 0.01$, is presented in Fig. 4 as a convex curve. There are 441 nodes, 760 internal pores, and 80 surface pores.

In the case of bulk blocking, fitting the theoretical curve of retention probability vs number of steps (*8*) on the random walk computer experiment results was very satisfactory in the whole range $0 \leq x_b \leq 1$. The performance of fitting is shown in Fig. 5 for three representative cases of low, medium, and heavy bulk pore blocking. It can be concluded that the random walk of a single particle in a blocked grid, with bulk pores blocked at random, is described accurately, within the whole blocking range, by the diffusion Eq. (6), making use of the concept of an effective diffusivity. The fitting error reaches a maximum at ~50% blocking; i.e., the case of a half-blocked grid, which is also a case of maximum heterogeneity, is the least satisfactorily described by the continuum diffusion equation.

Standard deviations in $\tilde{D}$ (see Fig. 4) also show a maximum at $x_b \simeq 50\%$. That is, the sensitivity of effective diffusivity to the exact topology of the grid is greatest in the case of a semiblocked grid. Indeed, a symmetry is expected between complementary cases of slight blocking, and heavy blocking. The former resembles the case of a totally unblocked grid, for which it is known that the single particle random walk process degenerates into the diffusion equation. In the latter, the grid consists of a continuum of blocked pores, interrupted by some unblocked pores, hence continuum theory is also very satisfactory. It is in the "transition" region of maximum heterogeneity (around 50%) that maximum uncertainty lies. The question of symmetry, and deviations from it, in relation to the assumptions

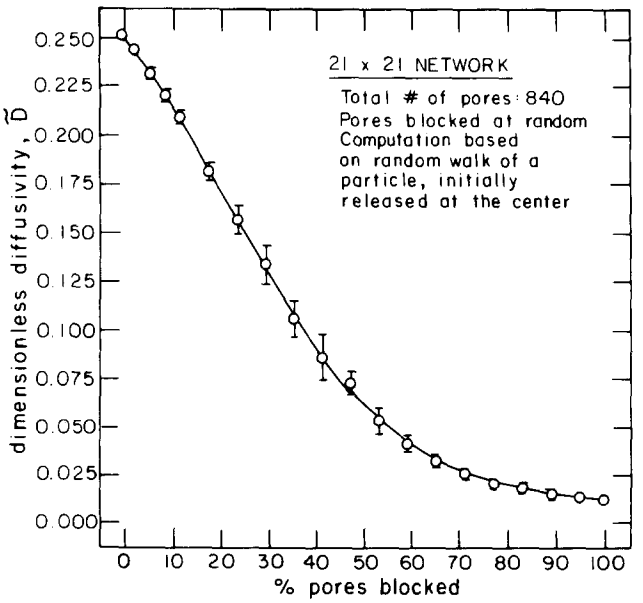

FIG. 4. Effect of bulk blocking of pores on diffusivity.

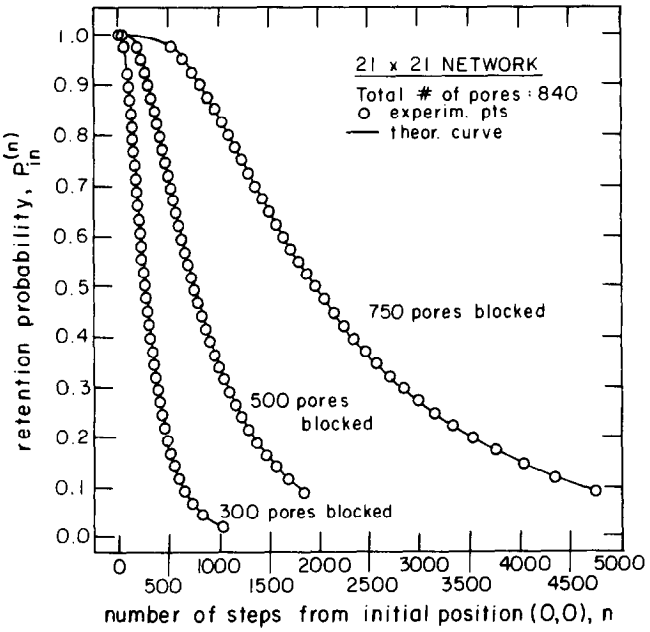

FIG. 5. Performance of fitting single particle random walk results in a bulk blocked grid by the theoretical expression (8).

made in this work, is further pursued in (*21*).

The dependence of effective diffusivity on the extent of bulk pore blocking, shown in Fig. 5, is highly nonlinear. The decay of $\tilde{D}$ with x_b could roughly be described as "quasiexponential." The variation of $\tilde{D}$ between the extreme values $\tilde{D}_0 = 0.2514$ and $\tilde{D}_1 = 0.0120$ as x_b varies from 0 to 1 is very satisfactorily correlated in the form

$$\frac{\tilde{D}}{\tilde{D}_1} = \left(\frac{\tilde{D}_0}{\tilde{D}_1}\right) \cdot \exp(0.991 - 0.144\, x_b - 2.257\, x_b^2 + 1.411\, x_b^3). \quad (9)$$

The numerical values of coefficients appearing in (9) probably depend on the particular value of b used. The general functional form (9), however, is believed to be characteristic of the changes in grid topology, brought about by bulk pore blocking.

b. Border Blocking

In this blocking mode, only pore entrances, or surface sites, along the crystal border are blocked at random. (The maximum number of blockings that can be introduced is thus $4(M + N)$.) Some examples of random blocking configurations generated in an 11 × 11 grid are given in Fig. 6. There are 121 nodes, of which 40 are surface nodes.

Here, blocking a surface site A is seen as a closing of the *entrance,* or neck, of the intracrystalline pore ending at A, just below the surface of the crystal (Fig. 7).

Transitions AC, CA from and to the interior of the crystal are hindered (probability reduced to b).

The transition probability for staying at C is increased by $\frac{1}{4} - b$.

The sorptive power of the blocked (or deactivated) site A is reduced. Once a particle reaches A, it will most likely (with probability $1 - 3b$) desorb and escape to the exterior of the crystal at the next step. The probability of transitions AB and AD is reduced to b.

Transitions BA and DA, which bring a particle to the blocked site by surface diffusion, are not affected.

In a border blocked grid, the particle can-

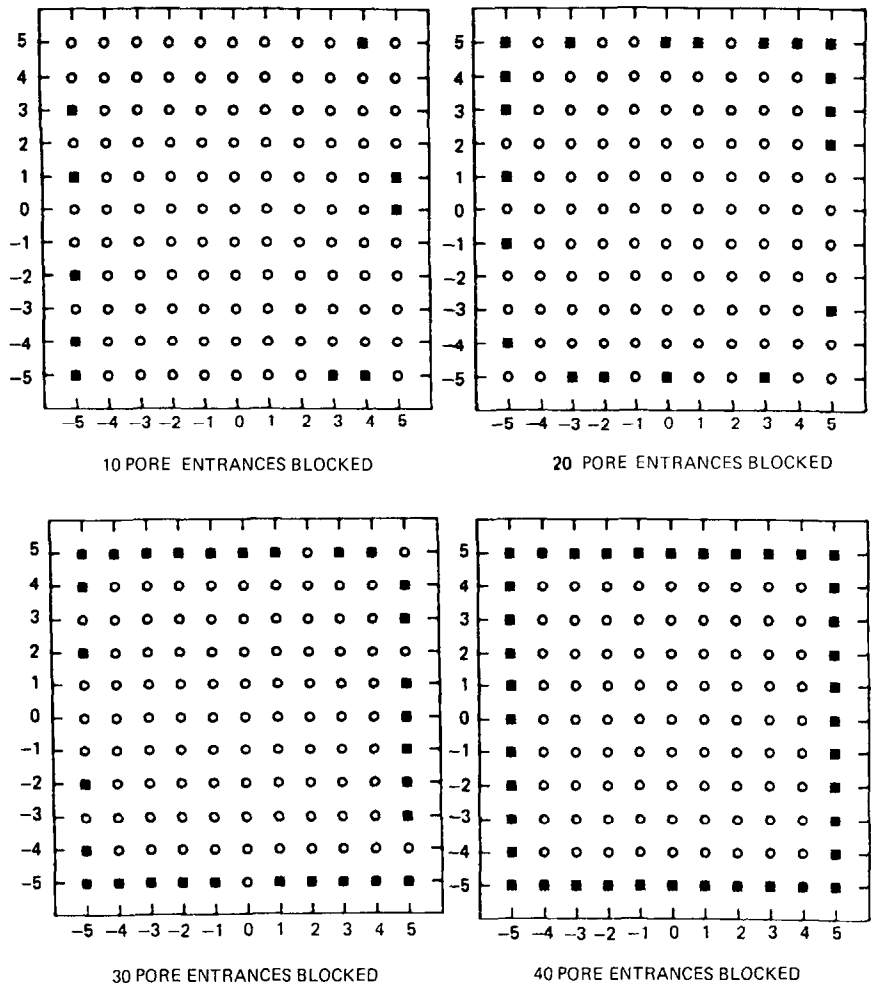

FIG. 6. Examples of random border blocking configurations in an 11 × 11 network.

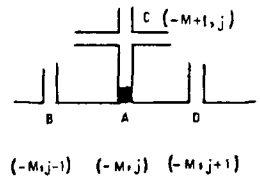

$p^{U}_{-M,j} = b$	$p^{D}_{-M+1,j} = b$	$p^{L}_{-M,j+1} = \frac{1}{4}$	$p^{R}_{-M,j-1} = \frac{1}{4}$
$p^{R}_{-M,j} = b$	$p^{S}_{-M+1,j} = \frac{1}{4} - b$	$p^{R}_{-M,j+1} = \frac{1}{4}$	$p^{L}_{-M,j-1} = \frac{1}{4}$
$p^{L}_{-M,j} = b$	$p^{U}_{-M+1,j} = \frac{1}{4}$	$p^{U}_{-M,j+1} = \frac{1}{4}$	$p^{U}_{-M,j-1} = \frac{1}{4}$
$p^{D}_{-M,j} = 1 - 3b$	$p^{L}_{-M+1,j} = \frac{1}{4}$	$p^{D}_{-M,j+1} = \frac{1}{4}$	$p^{D}_{-M,j-1} = \frac{1}{4}$
$p^{S}_{-M,j} = 0$	$p^{R}_{-M+1,j} = \frac{1}{4}$	$p^{S}_{-M,j+1} = 0$	$p^{S}_{-M,j-1} = 0$

FIG. 7. Changes in transition probabilities brought about by border site blocking.

not be altogether trapped until all pore entrances have been blocked. Thus, the case $b = 0.0$ can be examined. Two sets of results are presented here, obtained with $b = 0.0$ and $b = 0.01$.

The dependence of dimensionless diffusivity $\tilde{D} = D \cdot \tau/l^2$ on the extent of border blocking, as determined for a grid with $M = N = 10$, for the two b values studied, is given in Fig. 8 as a pair of concave curves.

The performance of fitting the retention probability vs number of steps relationship to compute values of $\tilde{D}$ is shown in Fig. 9 for three representative cases of slight, medium, and heavy border blocking. At low blocking percentages, the theoretical expression (8) describes the "experimental" $P_{in}^{(n)}$ relationship very satisfactorily. Fitting becomes worse, however, as the extent of blocking increases. This means that the continuum diffusion equation is no longer adequate for describing intracrystalline transport at high border blocking, and the concept of an effective diffusivity is less useful than in the case of bulk blocking, presented above.

The behavior of the $\tilde{D}(x_b)$ curves obtained for the two values of b examined is quite similar. In the limit $x_b \to 1.0$, the "experimental" $\tilde{D}(x_b)$ curve obtained with $b = 0.0$ correctly approaches the value $\tilde{D}_1 = 0.0$.

The nature of the $\tilde{D}(x_b)$ functionality, seen in Fig. 8, is strikingly different from that observed in the bulk blocking case (Fig. 4). The $\tilde{D}(x_b)$ curves are concave downward in the entire blocking range. Low extents of pore blocking are rather ineffective in reducing $\tilde{D}$, but the drop in diffusivity becomes steeper and steeper as the degree of blocking increases. As long as there exist enough unblocked sites along the border, a molecule reaching them can migrate, by surface diffusion, to the nonsorbing blocked sites, and from there readily escape to the surroundings. This moderates the decrease in $\tilde{D}$ brought about by the fact that blocked surface sites are not immediately accessible from the interior of the crystal. As the extent of surface blocking increases, the mechanism of escape via surface migration to a blocked site becomes less significant, hence the drop in $\tilde{D}$ more pronounced.

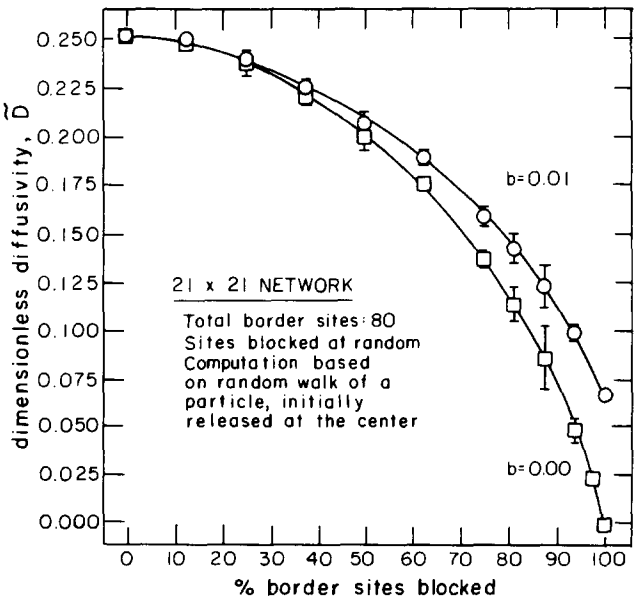

FIG. 8. Effects of border blocking on diffusivity.

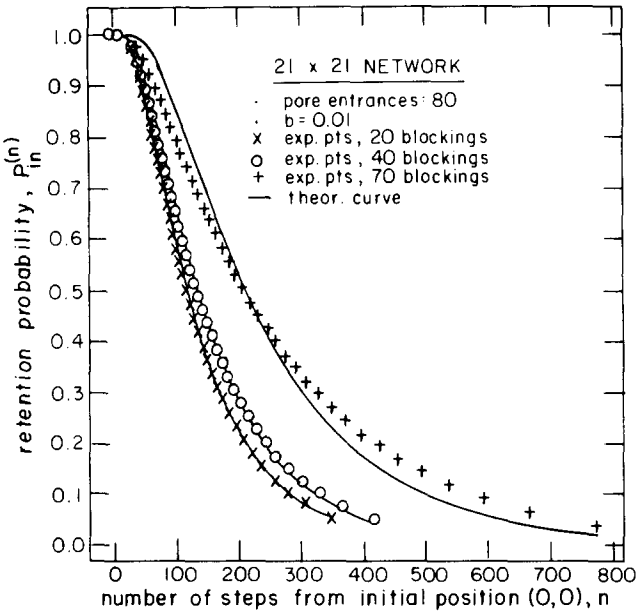

FIG. 9. Performance of fitting single particle random walk results in a border-blocked grid, by the theoretical expression (8).

Satisfactory analytical correlations of the experimental results were arrived at by use of the reduced diffusivity drop $(\tilde{D}_0 - \tilde{D})/(\tilde{D}_0 - \tilde{D}_1)$. In the case $b = 0.01$, results are correlated by the expression

$$\frac{\tilde{D}_0 - \tilde{D}}{\tilde{D}_0 - \tilde{D}_1} = 0.00104 - 0.0950\, x_b + 1.967\, x_b^2 - 2.517\, x_b^3 + 1.641\, x_b^4. \quad (10)$$

In the case $b = 0.0$, experimental results are described by

$$\frac{\tilde{D}_0 - \tilde{D}}{\tilde{D}_0 - \tilde{D}_1} = 0.00160 - 0.1280\, x_b + 2.079\, x_b - 3.078\, x_b^3 + 2.116\, x_b^4. \quad (11)$$

It is seen that the values of coefficients appearing in expressions (10) and (11) depend, to some extent, on b. However, the functional form expressed by (10) and (11) is quite similar, and is believed to be characteristic of the changes in grid topology brought about by border blocking.

II. OCCUPANCY EFFECTS

A stochastic model of diffusion and reaction in our simplified two-dimensional "crystal" was developed to study the effects of intracrystalline occupancy by mobile, sorbed reactant and product molecules (instead of the immobile blocking modifier molecules of the previous section) on the degree of transport limitations imposed on the reaction.

The reaction modeled is the simple isomerization A $\rightleftharpoons$ B in a crystal exposed to a bulk gaseous phase of pure A, where both the forward and the backward reactions are assumed to be first order, and the heat of reaction is assumed to be negligible.

In the stochastic approach, molecular behavior within the crystal is simulated by the Monte-Carlo method. A simulation experiment can be described as follows.

We start with a completely empty grid, and "bombard" it, at a constant rate, with A molecules from the outside. A molecules attach themselves to the border of the grid; they diffuse, by a random walk process, to the interior, where the reaction A $\rightleftharpoons$ B takes place at active sites, and ultimately exit the grid as A or B (converted) molecules. The number of molecules colliding

with, entering, reacting, present in, and exiting the grid is monitored at each step. It is evident that, by this technique, the situation in the grid is transient at the beginning. As more and more molecules enter and exit, the occupancy of the crystal by molecules is stabilized at a roughly constant level, and a steady state is attained. Simulation is interrupted at a predetermined number of steps N_S, after the system has operated for a sufficient time in the steady state. Results presented here are based on averaging over the last $N_S/2$ steps of the simulation. The fundamental interval elapsing between successive steps of the Monte-Carlo simulation is taken as equal to the diffusion step time of A, τ_A.

The following assumptions are made for particle entrance in the grid.

(*A.5*) The number of gas molecules colliding with the crystal border per time step is assumed to follow the Poisson distribution, with a parameter (mean) of λ collisions/step. It is by means of the value of λ that occupancy in the crystal is indirectly controlled.

(*A.6*) The spatial distribution of points of collision is uniform around the crystal border.

(*A.7*) A molecule is attached to the grid if the surface site on which it collides is unoccupied. Otherwise, it is deflected back into the gaseous phase.

Pore intersections are considered to be the catalytic sites within the crystal. The conversion process is governed by the following rules.

(*A.8*) All sites are assumed to be of equal activity. At a catalytic site, an A molecule has a fixed probability p of being converted into B within the time duration of a simulation step. The corresponding probability for the conversion B $\rightarrow$ A in the interval τ_A is q.

We symbolize by r_d the ratio of zero-occupancy diffusivities of species A and B:

$$r_d = \frac{D_A^0}{D_B^0} = \frac{\tau_B}{\tau_A}.$$

Movement of A and B molecules within the crystal channel system represented by the grid is modeled as a random walk process subject to assumptions (*A.1*) to (*A.4*). The presence of more than one molecules in the grid makes it necessary to introduce rules for particle interference during movement. As introduced here, these rules are independent of the identity of interfering particles, i.e., are the same for A–A, A–B, and B–B interactions. Interference between molecules is of a "hard sphere" type, stemming solely from changes in grid topology due to their physical presence. More specifically, the following assumptions are made.

(*A.9*) No more than one molecule can occupy a site at a given time.

(*A.10*) Molecules move through the pores in single file. Two molecules cannot bypass each other moving in opposite directions within a pore. For a system such as xylenes/ZSM-5, this assumption seems reasonable in view of the relative magnitudes of pore and molecular diameters.

(*A.11*) Movement from a site S_1 to a new site S_2, in a chosen direction $S_1 \rightarrow S_2$, occurs only if site S_2 is unoccupied. If site S_2 is occupied, the molecule stays in place (at S_1).

The sequencing and coordination of events used in the Monte-Carlo simulation is described in (*21*).

The parameters of the Monte-Carlo model of diffusion and reaction are M, N, λ, p, q, r_d. All results presented here were obtained with values of $M = 5$, $N = 5$, $p = 0.008$, $q = 0.005$, $r_d = 1.0$.

A *continuum formulation* of the problem, making use of the classical concepts of concentrations c_A, c_B (based on total crystal volume), intrinsic reaction rate constants k_1 (for reaction A $\rightarrow$ B), k_2 (for reaction B $\rightarrow$ A), and effective diffusivities D_A, D_B, was developed in parallel with the stochastic approach, for comparison purposes.

Under the assumptions (*A.10–A.12*), effective diffusivities, according to Riekert (*1*) are functions solely of the local occupancy,

$$\theta = \frac{c_A + c_B}{c_s} \tag{12}$$

where c_s is the saturation concentration of the crystal:

$$\begin{aligned} D_A &= D_A^0 \cdot (1 - \theta) \\ D_B &= D_B^0 \cdot (1 - \theta) \end{aligned} \tag{13}$$

In the continuum formulation, the crystal is viewed as a rectangular domain of dimensions L_x, L_y. The case $L_x = L_y = 2L$ is considered here (see Fig. 1). Due to symmetry, only the subdomain lying in the first quadrant of the (x, y) system needs be considered. The value of intracrystalline concentration of A along the crystal boundaries is specified as c_s.

The steady-state problem of reaction and diffusion can be cast into a dimensionless form, by use of the variables

$$X = \frac{x}{L}, \qquad Y = \frac{y}{L},$$

$$C = \left(1 + r_d \frac{k_2}{k_1}\right) \cdot \frac{c_A}{c_{A_i}} - r_d \cdot \frac{k_2}{k_1} = 1 - \left(\frac{1}{r_d} + \frac{k_2}{k_1}\right) \cdot \frac{c_B}{c_{A_i}}.$$

Let Θ denote the global occupancy in the crystal,

$$\Theta = \frac{\int_0^L \int_0^L (C_A + C_B)\, dxdy}{L^2 c_s}.$$

Let also $C_i = \frac{c_{A_i}}{c_s}$. The effectiveness factor can be determined from the dimensionless profile $C(X,Y)$ as

$$\eta = \int_0^1 \int_0^1 C dX dY. \tag{14}$$

In the special case of equal diffusivities, examined here ($r_d = 1$), occupancy is constant throughout the entire domain:

$$\theta(x, y) = \Theta = C_i \tag{15}$$

and the continuum problem assumes the simple *linear* form

$$\left.\begin{aligned} \nabla^2 C &= 2 \cdot \frac{\Phi^2}{1 - C_i} \cdot C \\ C(1, Y) &= C(X, 1) = 1 \\ \hat{x} \cdot \nabla C|_{(0,Y)} &= \hat{y} \cdot \nabla C|_{(X,0)} = 0 \end{aligned}\right\} \tag{16}$$

where Φ is the generalized Thiele modulus:

$$\Phi = \frac{L}{2}\left(\frac{k_1}{D_A^0} + \frac{k_2}{D_B^0}\right)^{1/2}. \tag{17}$$

Thus, the dimensionless solution and, by (14), the effectiveness factor, is a function of the single parameter

$$\Phi' = \frac{\Phi}{(1 - C_i)^{1/2}}$$

which is an effective generalized Thiele modulus, modified for occupancy effects.

An analytical solution of the problem (16) can be arrived at, following the method of Aris (*22*, p. 179). The result is

$$C(X, Y) = 1 - (\Phi')^2 \cdot \left(\frac{64}{\pi^2}\right) \cdot \sum_{m=1}^{\infty} \sum_{n=1}^{\infty} \left\{ \frac{(-1)^{m+n}}{(2m - 1)(2n - 1)} \cdot \frac{\cos[(m - \tfrac{1}{2})\pi X] \cdot \cos[(n - \tfrac{1}{2})\pi Y]}{4(\Phi')^2 + [(m - \tfrac{1}{2})^2 + (n - \tfrac{1}{2})^2]\pi^2} \right\} \tag{18}$$

from which (14)

$$\eta = 1 - (\Phi')^2 \cdot \left(\frac{16}{\pi^2}\right)^2 \sum_{m=1}^{\infty} \sum_{n=1}^{\infty} \left\{ \frac{1}{(2m - 1)^2 \cdot (2n - 1)^2} \cdot \frac{1}{4(\Phi')^2 + (m - \tfrac{1}{2})^2\pi^2 + (n - \tfrac{1}{2})^2\pi^2} \right\}. \tag{19}$$

A plot of the function $\eta(\Phi')$, in the familiar logarithmic coordinates, is given in Fig. 10.

Under constant Φ, the solution of (16) gives η as a function of $\Theta = C_i$, i.e., provides a direct quantitative expression of the effects of occupancy on the degree of diffusional limitations. The function $\eta(\Theta)$ for a value of $\Phi = 0.6841$ (= value corresponding to the Monte-Carlo simulation) is given in Fig. 11 (continuous line).

One can establish a correspondence between the parameters of the stochastic model, and those of the continuum ap-

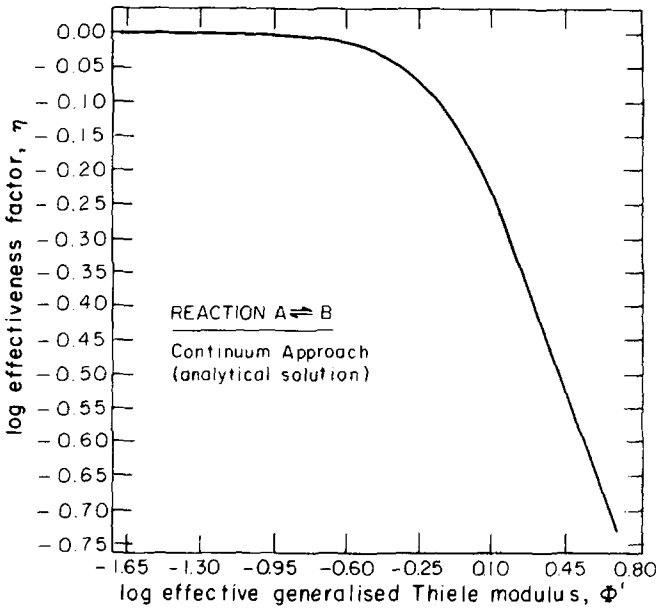

FIG. 10. Effectiveness factor η as a function of the effective generalized Thiele modulus Φ', according to the continuum approach.

proach. The two-dimensional random walk process of A and B in the crystal grid is equivalent to a continuum diffusion process in an "extended" domain, of dimensions $2(N + 1)l \times 2(M + 1)l$ (see I) with

$$D_A^0 = \frac{l^2}{4\tau_A}, \qquad D_B^0 = \frac{l^2}{4\tau_B} = \frac{1}{r_d} \cdot \frac{l^2}{4\tau_A}. \quad (20)$$

Intrinsic reaction rate constants can be defined in terms of p, q, and τ_A as

$$k_1 = \frac{p}{\tau_A}, \qquad k_2 = \frac{q}{\tau_A}. \quad (21)$$

Thus, the generalized Thiele modulus can be expressed in terms of the stochastic model parameters (*21*) as

$$\Phi = 2\frac{[M \cdot N \cdot (M + 1) \cdot (N + 1)]^{1/2}}{M + N}\{p + r_d q\}^{1/2}. \quad (22)$$

For the parameter values used in the Monte-Carlo simulation, Φ is equal to 0.6841. By the continuum formulation (Eq. (19)) this corresponds to a zero occupancy value of the effectiveness factor equal to

$$\eta|_{\Theta=0} = 0.8062. \quad (23)$$

In the stochastic model, global occupancy is determined, in a straightforward manner, from the "observables" of Monte-Carlo simulation, as

$$\Theta = \frac{\bar{N}_A + \bar{N}_B}{(2M + 1) \cdot (2N + 1)} \quad (24)$$

where $\bar{N}_A$, $\bar{N}_B$ denote the average number of A, respectively B, molecules present in the crystal at steady state.

Meaningful definitions of the effectiveness factor in terms of the Monte-Carlo observables can be arrived at by analogy to the classical (continuum) reaction and diffusion theory. Three alternative definitions used in this work (20) are

$$\eta_1 = \frac{r_d}{p} \cdot \frac{\bar{N}_{B,ex}}{r_d\bar{N}_A + \bar{N}_B}$$

$$\eta_2 = \frac{r_d}{p} \cdot \frac{\bar{N}_{B,ex}}{r_d\bar{N}_A + \frac{1}{q}(p\bar{N}_A - \bar{N}_{B,ex})} \quad (25)$$

$$\eta_3 = \frac{r_d}{p} \cdot \frac{p\bar{N}_A - q\bar{N}_B}{r_d\bar{N}_A + \bar{N}_B}$$

where $\bar{N}_{B,ex}$ denotes the average number of

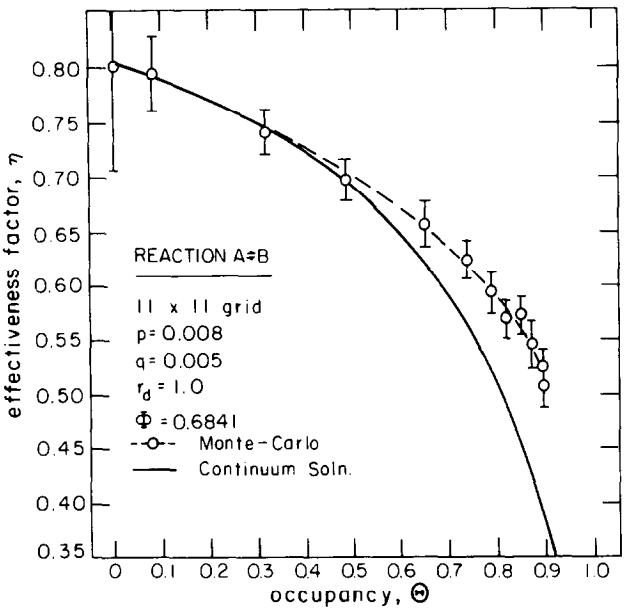

FIG. 11. Variation of effectiveness factor with global occupancy (comparison between Monte Carlo and continuum approaches).

B molecules exiting the crystal per simulation step of duration τ_A.

Notice, that the definitions of η_1, η_2, η_3 are equivalent, as long as the fundamental steady-state balance

$$\bar{N}_{B,ex} = p\bar{N}_A - q\bar{N}_B \qquad (26)$$

is satisfied.

In practice, fluctuations in random number generation lead to small differences between the values of η_1, η_2, η_3. Effectiveness factors presented in the following are averages of the three values obtained from simulation experiments by Eqs. (25).

Some results, obtained by Monte-Carlo simulation of diffusion and reaction, for the abovementioned values of M, N, p, q, r_d, and λ ranging from 0.1 to 1000, are presented in Figs. 11 and 12. Bars denote standard deviations, due to fluctuations inherent in the stochastic model. Figure 12 gives the number of A, B, and total molecules in the grid as a function of collision frequency. (For values of $\lambda > 200$, all three curves become practically horizontal.) The functional relationship $\Theta = \Theta(\lambda)$, which can be directly obtained from the results of Fig. 12, is an expression of the equilibrium "sorption isotherm" followed by our model zeolite. Analysis of the simulation results (*21*) shows that, up to occupancies of 80%, sorption conforms to a Langmuir isotherm, as can be predicted on the basis of model assumptions.

Figure 11 shows the variation of effectiveness factor with intracrystalline occupancy according to the Monte-Carlo model (points and broken line), i.e., it is a quantitative expression of diffusional limitations due to molecule interference at high occupancies. Notice that the zero-occupancy limit value of η determined by Monte-Carlo simulation agrees very well with the value (23) predicted by continuum theory. In general, Monte-Carlo and continuum results show good agreement in the region $\Theta <$ 50%. As occupancy is further increased, Monte-Carlo values of η tend to be higher than continuum values determined by (19) for the same value of Θ, i.e., the discrete model predicts a situation somewhat less diffusion limited than the continuum model.

From the results of Monte-Carlo simulation it is evident that, at large values of λ, a

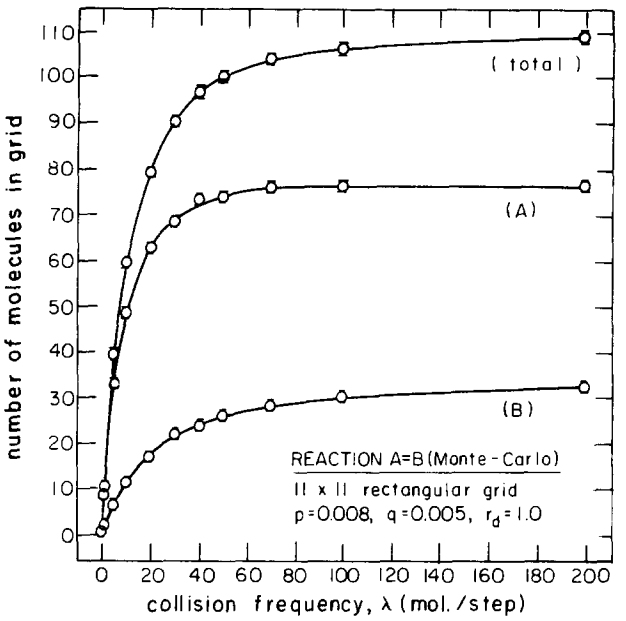

FIG. 12. Monte Carlo model: number of particles in grid as a function of collision frequency.

"limiting," or saturation situation is reached, at which phenomena occurring in the catalyst are not influenced by further increases in the collision frequency λ. This is to be expected on the basis of the finite capacity of our crystal for molecules. What is, perhaps, the most striking result of the Monte-Carlo approach is that, in this "saturation" situation, the limiting occupancy attained in the grid is less than 100%. Under saturation conditions ($\lambda \to \infty$), Θ within a simulation step fluctuates between a minimum of 0.90 (directly after molecular escape) and a maximum of 0.97 (immediately after molecular attachment at the border). Close examination reveals that, even for $\lambda \to \infty$, there exist unoccupied sites in the interior of the crystal (on the average 3.1 internal unoccupied sites for an 11 × 11 crystal). The existence of internal vacancies under saturation conditions can be understood, if one considers the phenomenon of simultaneous movement of groups of two or more molecules, residing in adjacent rows on and parallel to the crystal border, toward the exterior of the crystal. Such "group migrations" occur with a finite probability in the stochastic model, and are obviously equivalent to migration of vacancies towards the interior of the crystal.

Under saturation conditions, the effectiveness factor assumes a nonzero value of $\eta_\infty \simeq 0.51$.

The existence of a limiting situation at which $\Theta_\infty < 1$ and $\eta_\infty > 0$ evidently differentiates the Monte-Carlo from the continuum approach, according to which a situation of full occupancy, at which the effectiveness factor drops to zero, is attainable.

The continuum and the stochastic approaches developed here to examine occupancy effects rest on essentially the same assumptions. The lack of complete equivalence between them is rather due to differences in the fundamental picture of the situation employed by each model.

In the continuum model, catalytic activity is uniformly distributed over the whole crystal (domain) instead of residing at specific sites. Notice, in particular, the difference in the notion of "surface" between the two models. In the spatially and temporally discrete stochastic model, the surface is a set of sites of finite catalytic activity,

which can sustain a reaction even in the case of extreme diffusion control, where incoming molecules cannot penetrate at all into the crystal. In the continuum model, the surface is but a mathematical borderline. Conditions of extreme diffusion control would cause the reactant gas to be confined to an infinitesimal strip of catalyst volume near the surface, of an accordingly infinitesimal catalytic activity, i.e., they would cause the reaction rate to drop to zero.

With reference to the limiting occupancy situation predicted by the stochastic model, we note the following:

The particular limiting values assumed by model parameters as $\lambda \to \infty$ are functions of the grid size. In fact, the whole concept of a limiting steady state situation with $\Theta_\infty < 1$ seems to be a result of the "finiteness" of the grid. As the crystal becomes larger and larger ($M \to \infty$, $N \to \infty$) the number of surface sites becomes insignificant in comparison with the total number of sites, and the diffusion and reaction behavior at high occupancies is expected to move closer to the results of continuum theory.

It is evident that, in the limit of high occupancies, the situation becomes extremely sensitive to phenomena occurring at the surface of the crystal. Thus, any model attempting to account for high occupancy behavior should incorporate sound and carefully tested assumptions regarding the phenomena of sorption, surface diffusion, and reaction on surface borders.

III. MONTE-CARLO INVESTIGATION OF BORDER-BLOCKING EFFECTS

The Monte-Carlo model presented above was applied to the reaction and diffusion situation in a grid, in which a fraction of the surface sites has been randomly blocked. The objective was to study how the observed reaction rate and the degree of diffusional limitations vary with the extent of border blocking.

There exist several interrelated factors, stemming from border blocking, which influence the intracrystalline reaction and dif-

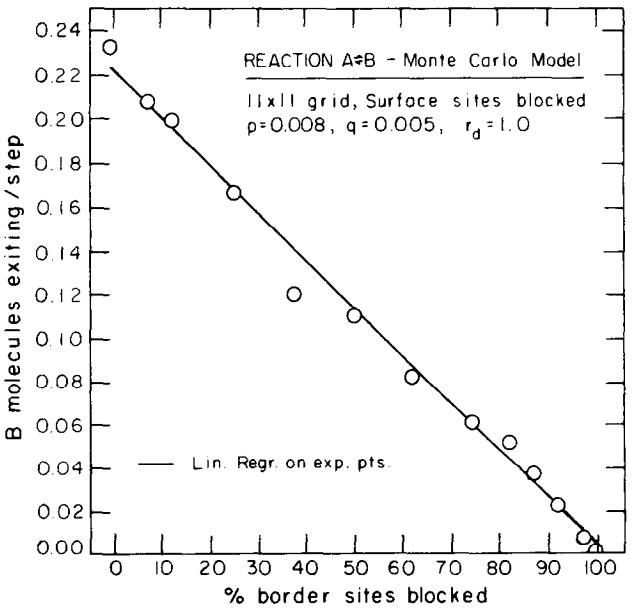

FIG. 13. Monte Carlo simulation of diffusion and reaction in a border blocked grid: observed reaction rate vs degree of border blocking.

fusion situation. One can classify them as follows:

(i) Decrease in the rate of entrance of A particles from the gaseous phase into the crystal, due to unavailability of pore entrances.

(ii) Increase in the "tortuosity" of diffusion paths due to surface blocking (see I).

(iii) Decrease in the intrinsic catalytic activity of the crystal, due to the fact that blocked sites do not act any more as catalytic sites (blocking is a form of poisoning).

(iv) Decrease in occupancy Θ with increasing degree of blocking (this phenomenon is related to (i) and (ii)).

We thus have a rather complex situation, for which no simple corresponding continuum formulation exists, and a stochastic approach is perfectly justified.

Assumptions as to the effects of border blocking on molecular transport in the grid were identical to those used in (I).

Results presented here were obtained from a series of simulation runs in an 11 × 11 grid, keeping the collision frequency constant at $\lambda = 5$ molecules/step, and varying the number of blocked surface sites from $N_b = 0$ ($x_b = 0.0$) to $N_b = 39$ ($x_b = 0.975$). (This corresponds to studying the catalytic performance of a crystal under constant temperature and pressure, but at varying degrees of structural modification.)

The rate of exit of B particles from the crystal grid ($\bar{N}_{B,ex}$) was chosen as a representative measure of the observed reaction rate. Figure 13 shows an approximately linear decrease of reaction rate with border blocking, toward the value 0.0 at $x_b = 1.0$.

The experimental $\eta(x_b)$ functionality, as determined by Monte-Carlo, is shown in Fig. 14. Note that, with the value of λ used, there already exist appreciable occupancy effects in the unblocked grid ($\Theta = 0.32$ at $x_b = 0.0$). In the region of low degrees of border blocking, η is seen to remain practically constant. Indeed, the effects of blocking on diffusivity are slight in this region (Fig. 8), whereas occupancy limitations gradually subside with increasing x_b. The $\eta(x_b)$ curve is concave downward, dropping smoothly toward the expected value of $\eta = 0$ at $x_b = 1.00$.

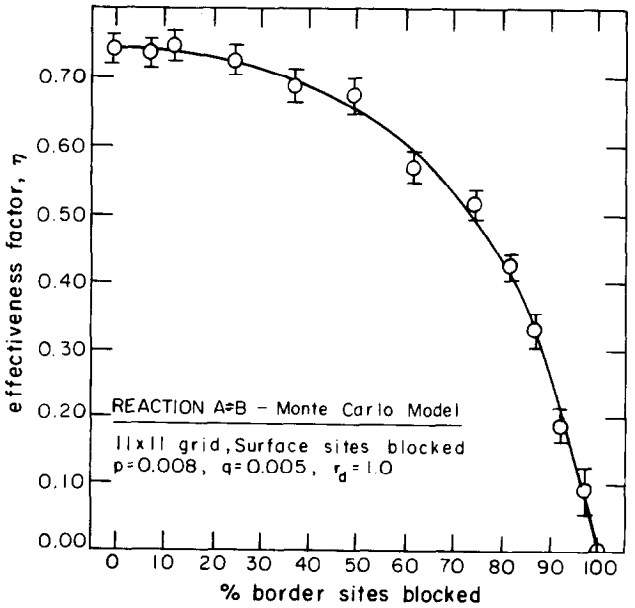

FIG. 14. Monte Carlo simulation of diffusion and reaction in a border blocked grid: effectiveness factor vs degree of border blocking.

CONCLUSIONS

Structural modifications of shape selective zeolite catalysts, thought to cause partial blocking of the intracrystalline pore system, bring about a decrease in the transport rate of sorbed species in the catalyst. The behavior of intracrystalline diffusivity is quite sensitive to the blocking mode used, being distinctly different in the two extreme cases of bulk blocking and border blocking. This could prove useful in resolving questions related to the structure of several modified shape selective forms of zeolite catalysts used today.

Monte-Carlo simulation can be an efficient and self-consistent method for attacking problems of transport and reaction in microporous solids. Although lacking in "accuracy" and expensive in computing time, it is very flexible. Moreover, it can point out characteristics immediately related to the "finiteness" of the intracrystalline pore system and not predictable by alternative continuum approaches. In view of the complex, discrete topology of zeolite channel systems, stochastic modeling seems to be an approach particularly suitable for understanding structure–selectivity relationships in zeolite catalysis.

NOMENCLATURE

b	Probability of passing through a blocked pore
c	Intracrystalline concentration (kmol/m^3 crystal)
C	Dimensionless concentration, used in continuum formulation
c_{A_i}	Value of intracrystalline concentration of A at the surface of the crystal (kmol/m^3 crystal)
C_i	Surface intracrystalline concentration, nondimensionalized with respect to saturation concentration, $C_i = c_{A_i}/c_S$
c_S	Saturation value of intracrystalline concentration (kmol/m^3 crystal)
D	Effective intracrystalline diffusivity (m^2/sec)
$\tilde{D}$	Dimensionless effective diffusivity from random walk experiments, $\tilde{D} = D \cdot \tau/l^2$
k_1	Rate constant for reaction $A \rightarrow B$ (sec^{-1})
k_2	Rate constant for reaction $B \rightarrow A$ (sec^{-1})
l	Distance between successive pore intersections (sites) of crystal grid in stochastic approach (m)
L	Half side length of the square domain representing the crystal in continuum approach (m)
L_x, L_y	Side lengths of the rectangular domain representing the crystal in the continuum approach (m)
M	Grid size parameter: number of nodes in the "vertical" direction is $(2M + 1)$
n	Step number in random walk experiments
N	Grid size parameter: number of nodes in the "horizontal" direction is $(2N + 1)$
N_b	Number of blocked pores, or number of blocked surface sites
N_j	Number of molecules of species j in the grid
$N_{j,ex}$	Number of molecules of species j exiting the crystal per step
N_s	Number of Monte-Carlo simulation steps
p	Probability of conversion $A \rightarrow B$ per site per simulation step in Monte-Carlo approach
$P_{i,j}^{(n)}$	Probability of being at site (i, j) at the nth random walk step
$p_{i,j}^R$, $p_{i,j}^L$, $p_{i,j}^U$, $p_{i,j}^D$, $p_{i,j}^S$	Transition probabilities for moving right, left, up, down, and staying at the same place, respectively, for site (i, j)
$P_{in}^{(n)}$	Probability of being in the grid at step n of random walk
q	Probability of the conversion $B \rightarrow A$ per site per simulation step time in Monte-Carlo approach

r_d	Ratio of zero-occupancy diffusivity of species A to species B; $r_d = D_A^0/D_B^0$
t	Time (sec)
x	"Horizontal" spatial coordinate in the plane of the grid (m)
X	Dimensionless horizontal coordinate, $X = x/L$
$\hat{x}$	Unit vector in x-direction
x_b	Fraction of blocked pores, or fraction of blocked surface sites
y	"Vertical" spatial coordinate in the plane of the grid (m)
Y	Dimensionless vertical coordinate, $Y = y/L$
$\hat{y}$	Unit vector in y-direction

Greek Symbols

δ	Dirac delta function
η	Effectiveness factor
θ	Local occupancy
Θ	Global occupancy
λ	Mean frequency of molecular collisions with crystal surface (molecules/step)
τ	Diffusion step time (sec)
Φ	Generalized Thiele modulus, defined in terms of crystal volume-to-external area ratio
Φ'	Generalized Thiele modulus, modified for occupancy effects

Superscripts

$-$	Mean value
^{0}	Zero occupancy

Subscripts

A	Species A
B	Species B
0	Zero blocking
1	Full blocking
∞	Limiting condition $\lambda \to \infty$

REFERENCES

1. Riekert, L., *in* "Advances in Catalysis" (D. D. Eley, H. Pines, and P. B. Weisz, Eds.), Vol. 21, p. 281. Academic Press, New York, 1970.
2. Weisz, P. B., *in* "New Horizons in Catalysis" (T. Seiyama and K. Tanabe, Eds.), No 7A, p. 3. Elsevier, Amsterdam, 1980.
3. Derouane, E. G., *in* "Catalysis by Zeolites" (B. Imelik, C. Naccache, Y. Ben Taarit, J. C. Vedrine, G. Coudurier, and H. Praliaud, Eds.), Vol. 5, p. 5, Elsevier, Amsterdam, 1980.
4. Kaeding, W. W., Chu, C., Young, L. B., Weinstein, B., and Butter, S. A., *J. Catal.* **67,** 159 (1981).
5. Young, L. B., Butter, S. A., and Kaeding, W. W., *J. Catal.* **76,** 418 (1982).
6. Kaeding, W. W., Chu, C., Young, L. B., and Butter, S. A., *J. Catal.* **69,** 392 (1981).
7. Chen, N. Y., Kaeding, W. W., and Dwyer, F. G., *J. Amer. Chem. Soc.* **101,** 6783 (1979).
8. Wei, J., *J. Catal.* **76,** 433 (1982).
9. Dejaifve, P., Auroux, A., Gravelle, P. C., and Vedrine, J. C., *J. Catal.* **70,** 123 (1981).
10. Vedrine, J. R., Auroux, A., Dejaifve, P., Ducarme, V., Hoser, H., and Zhou, S., *J. Catal.* **73,** 147 (1982).
11. Dessau, R. M., *in* "Adsorption and Ion Exchange with Synthetic Zeolites" (W. H. Flank, Ed.), ACS Symposium Series No 135, p. 123. Washington, D.C., 1980.
12. Haag, W. O., Lago, R. M., and Weisz, P. B., Faraday General Discussion No 72, September 14–16, 1981, at the University of Nottingham, England.
13. Kokotailo, G. T., Lawton, S. L., Olson, D. H., and Meier, W. M., *Nature (London)* **272,** 437 (1978).
14. Meier, W. M., and Olson, D. H., "Atlas of Zeolite Structure Types." Published by the Structure Commission of the International Zeolite Association, Zurich, 1978.
15. Olson, D. H., Kokotailo, G. T., Lawton, S. L., and Meier, W. M., *J. Phys. Chem.* **85,** 2238 (1981).
16. Barrer, R. M., and Jost, W., *Trans. Faraday Soc.* **45,** 928 (1949).
17. Barrer, R. M., and Rees, L. V., *Trans. Faraday Soc.* **50,** 852 (1952) and **50,** 989 (1952).
18. Ruthven, D. M., *Canad. J. Chem.* **52,** 3523 (1974).
19. Topsoe, N. Y., Pedersen, K., and Derouane, E. G., *J. Catal.* **70,** 41 (1981).
20. Carslaw, H. S., and Jaeger, J. C., "Conduction of Heat in Solids," 2nd Ed. Clarendon Press, Oxford, 1959.
21. Theodorou, D. N., S. M. Thesis, Massachusetts Institute of Technology, 1983.
22. Aris, R., "The Mathematical Theory of Diffusion and Reaction in Permeable Catalysts," Vol. I. Clarendon Press, Oxford, 1975.